Electronic Supplementary Material (ESI) for Nanoscale Horizons.

Electronic Supplementary Information

Highly efficient electrocatalytic biomass valorization over perovskite-derived nickel phosphide catalyst

Wanbing Gong,[a] Jiayi Li,[a] Jun Ma,[a,b] Dong Liu,*[a,b] Ran Long[a] and Yujie Xiong*[a]

[a] Hefei National Research Center for Physical Sciences at the Microscale, School of Chemistry and Materials Science, National Synchrotron Radiation Laboratory, University of Science and Technology of China, Hefei, Anhui 230026, P. R. China.

[b] Suzhou Institute for Advanced Research, University of Science and Technology of China, Suzhou, Jiangsu 215123, P. R. China.

Address correspondence to yjxiong@ustc.edu.cn; dongliu@ustc.edu.cn.

Catalysts preparation

In a typical experiment, NF (2 × 3 cm) was immersed in 2.0 M HCl solution to remove the nickel oxides and then rinsed with deionized water. The precursor solution was prepared by dissolving 1 mmol $La(NO_3)_3 \cdot 6H_2O$, 1 mmol $Ni(NO_3)_2 \cdot 6H_2O$ and 14 mmol KOH in 40 mL of deionized water, followed by transferring into a Teflon-lined autoclave (50 mL) with NF. Afterwards, the reaction was maintained at 160 °C for 8 h to prepare the $LaNiO_3$ based precursor (LN). Finally, the LN was taken out, washed and vacuum dried at 60 °C.

The LN was thermally treated at 400 ^oC for 2 h with a ramping rate of 2 °C min^{-1} in Ar atmosphere to obtain LN-400 electrode. After that, the LN-400 sample was placed in a small crucible, which was put into a big crucible containing 200 mg $NaH_2PO_2 \cdot H_2O$ in a tube furnace. The reaction was performed at different calcination temperatures 350 ^oC for 4 h with a ramping rate of 2 °C min^{-1} in N_2 atmosphere to obtain LN-400-P-350 electrode.

Catalysts characterization

Scanning electron microscopy (SEM) images of the samples were taken on a FESEM (SU8020) operated at an accelerating voltage of 10.0 kV. Transmission electron microscopy (TEM, JEOL-2010) was operated at an acceleration voltage of 200 kV. Scanning transmission electron microscopy (STEM) images of the samples were recorded by a high resolution TEM (Philips TecnaiG2 F20) operated at an acceleration voltage of 200 kV. Powder X-ray diffraction (XRD) patterns were analyzed on a Philips X-Pert Pro X-ray diffractometer with using the Ni-filtered monochromatic Cu Kα radiation ($\lambda K_{\alpha 1}$ = 1.5418 Å) at 40 keV and 40 mA. XPS analysis was performed on an ESCALAB 250 X-ray photoelectron spectrometer (Thermo, USA) equipped with Al $K_{\alpha 1,2}$ monochromatized radiation at 1486.6 eV X-ray source. The *in situ* Raman spectra of the samples were recorded on a WITec alpha 300R confocal Raman microscope with 532 nm excitation laser in a custom-built H-type PTFE electrochemical cell. The metal contents were determined by the inductively coupled plasma spectroscopy (ICP 6300, Thermo Fisher Scientific).

Electrochemical measurements

All electrochemical measurements were operated in a H-type electrochemical cell with anode and cathode chambers separated by a Nafion proton exchange membrane. The electrochemical tests were performed on an electrochemical station (CHI 660E) with as-synthesized sample as the working electrode, and a Hg/HgO electrode and a Pt wire electrode as the reference and counter electrode, respectively. Prior to experiment, the electrolyte was bubbled with N_2 for 0.5 h so that the air was removed completely. In a typical experimental, linear sweep voltammetry (LSV) was conducted at a scan rate of 10 mV s^{-1} before and after the addition of 5-hydroxymethylfurfural (HMF) into the anodic compartment. The impedance spectra were recorded using potentiostatic mode over a frequency range

from 1 to 10^5 Hz (5 mV AC dither) at 1.49 V vs. RHE. The non-faradaic potential range is 1.19 to 1.29 V vs. RHE for C_{dl} test. The electrochemical HMF oxidation were conducted in 20 mL of 1.0 M KOH solution and stirred at ~500 rpm with a magnetic stir bar at room temperature. For the analysis of products, 10 µL of the electrolyte solution was withdrawn from the electrolyte solution and diluted with 10 mL water, which was then analyzed using high-performance liquid chromatography (HPLC, Waters 1525). The HPLC was equipped with an ultraviolet−visible detector set at 265 nm and a 4.6 mm × 150 mm Shim-pack GWS 5 µm C 18 column. A mixture of eluting solvents (A and B) was utilized. Solvent A was 5 mM ammonium formate aqueous solution and solvent B was methanol. Separation and quantification were accomplished using an isocratic elution of 70% A and 30% B for 10 min run time and the flow rate was set at 0.5 mL min^{-1}. The identification and quantification of the products were determined from the calibration curves by applying standard solutions with known concentrations of commercially purchased pure reactants, intermediates, and final products. The conversion, yield and Faradaic efficiency (FE) was estimated using the following equations:

$$Conversion = \left(1 - \frac{mol\ of\ reactant\ after\ reaction}{mol\ of\ reactant\ taken\ initially}\right) \times 100\% \quad (1)$$

$$Yield = \frac{mol\ of\ each\ product}{mol\ of\ reactant\ taken\ initially} \times 100\% \quad (2)$$

$$FE = \frac{mol\ of\ \ product\ formed}{total\ charge\ passed\ /\ (n * F)} \times 100\% \quad (3)$$

where n is the number of electron transfer for each product and F is the Faraday constant (96485 C mol^{-1}).

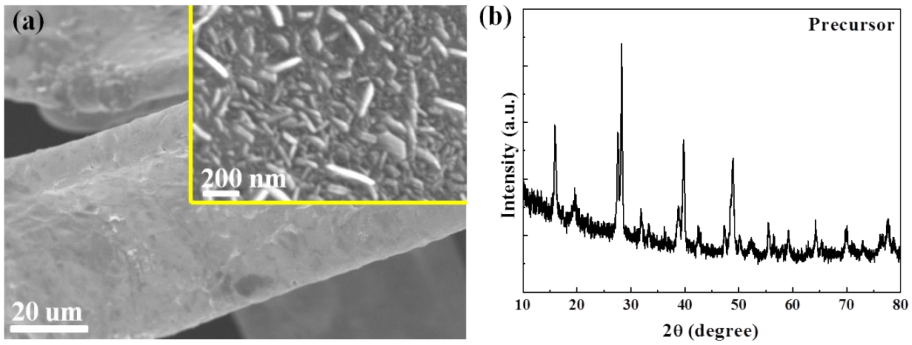

Fig. S1. The corresponding (a) SEM image (Inset: high magnification image) and (b) XRD pattern of precursor.

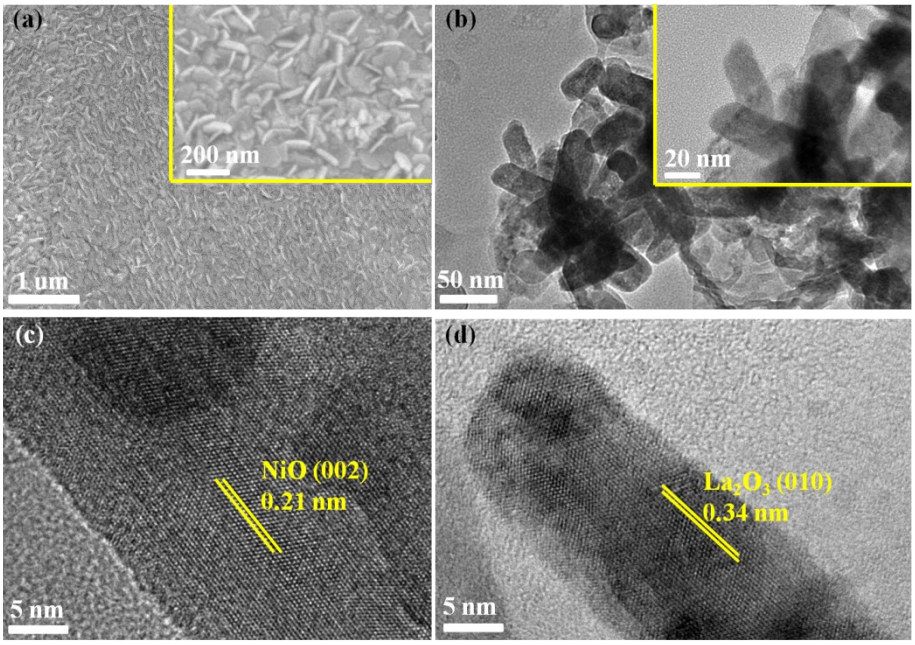

Fig. S2. The corresponding (a) SEM image (Inset: high magnification image), (b) TEM image (Inset: high magnification image) and (c-d) HRTEM images of LN-400.

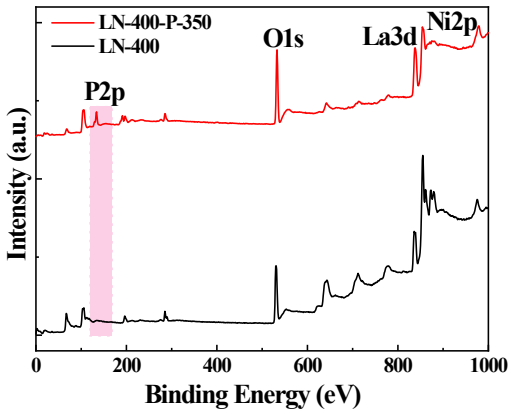

Fig. S3. The XPS survey spectra of LN-400 and LN-400-P-350 catalysts.

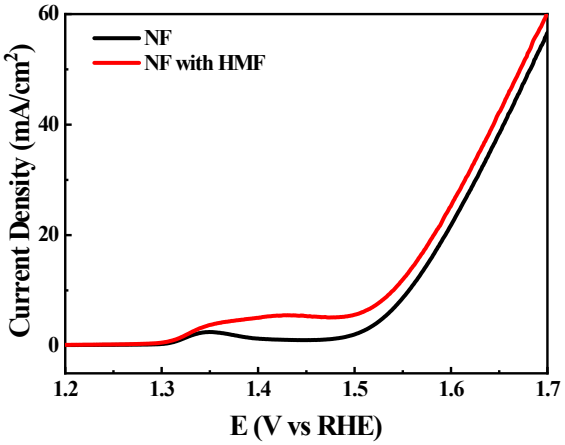

Fig. S4. The LSV curves of NF in 1.0 M KOH without and with 10 mM HMF.

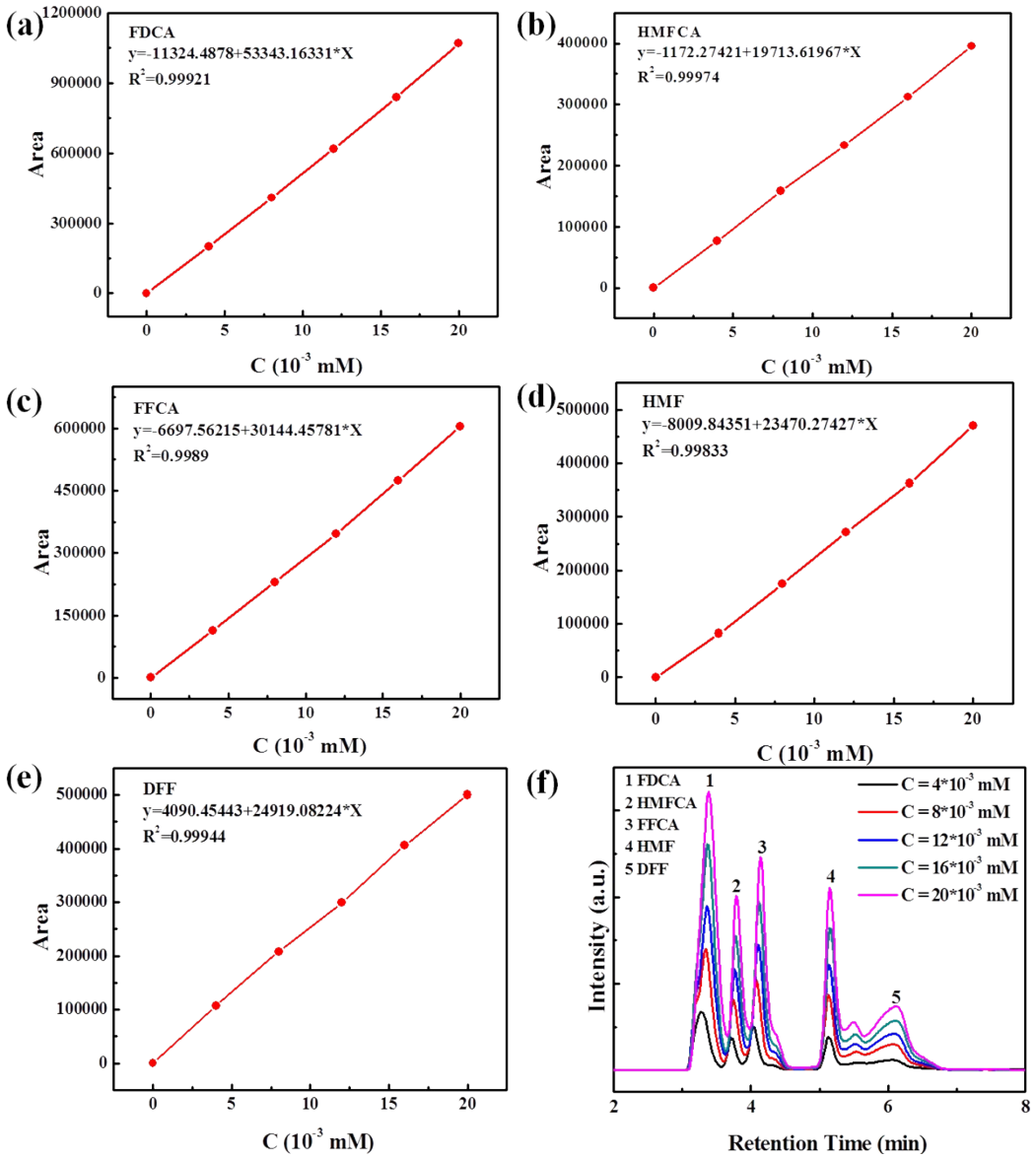

Fig. S5. Standard HPLC calibration curves of (a) FDCA, (b) HMFCA, (c) FFCA, (d) HMF and (e) DFF; (f) HPLC chromatograms of standard HMF, FDCA and other intermediates with various concentrations.

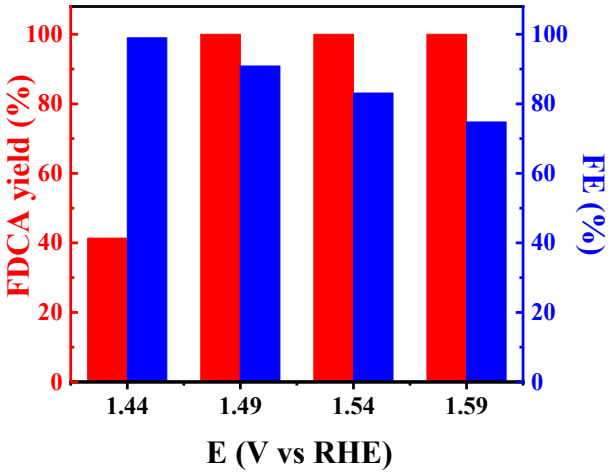

Fig. S6. FDCA yields and FEs of under different potentials.

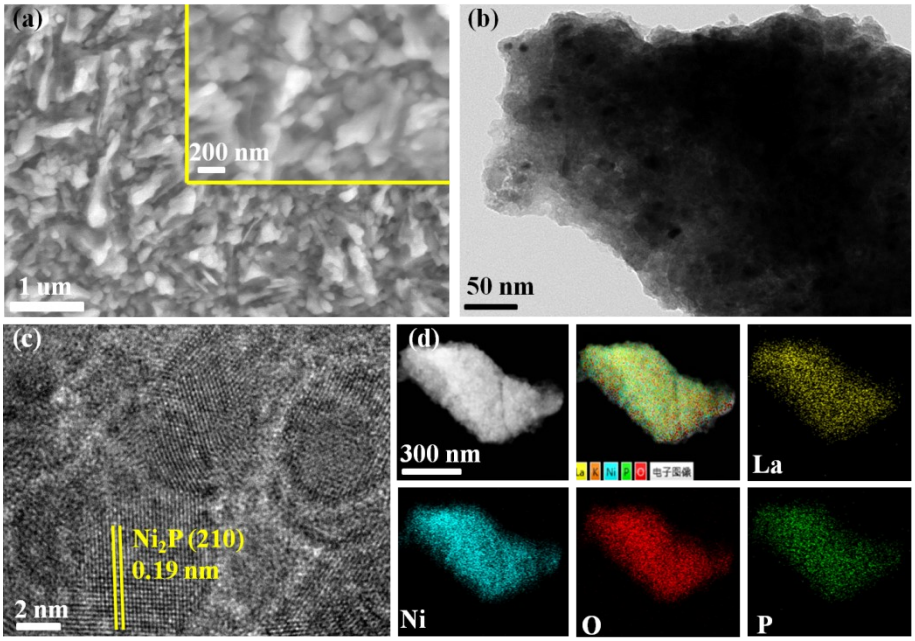

Fig. S7. (a) SEM image (Inset: high magnification SEM image); (b) TEM image; (c) HRTEM image; (d) HAADF-STEM image and elemental mapping images of LN-400-P-350 catalyst after 5 cycles.

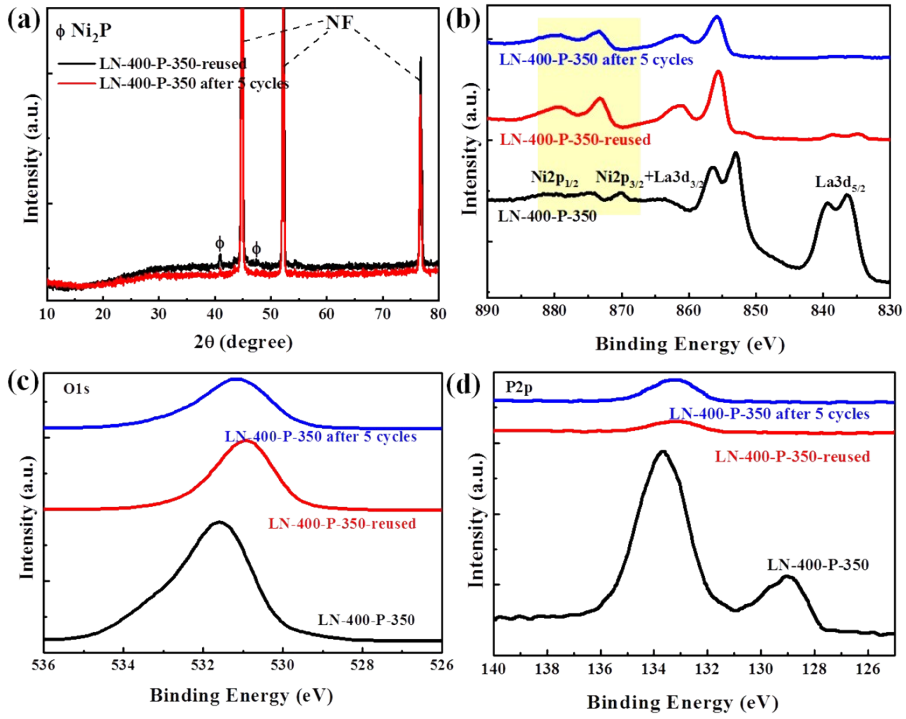

Fig. S8. (a) XRD patterns; (b) High resolution La 3d + Ni 2p spectra; (c) O 1s spectra and (d) P 2p spectra of LN-400-P-350-reused and LN-400-P-350 after 5 cycles catalysts.

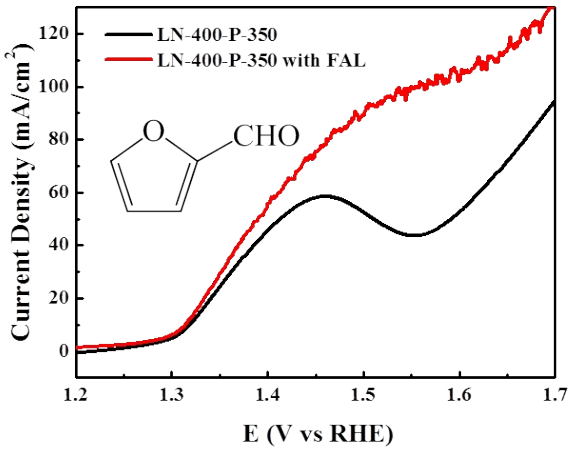

Fig. S9. LSV curves of LN-400-P-350 in 1.0 M KOH without and with 10 mM FAL.

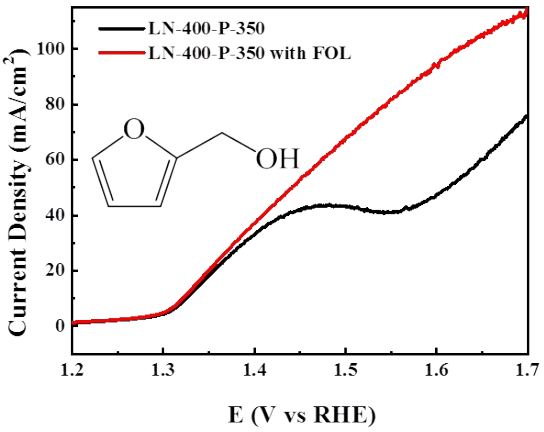

Fig. S10. LSV curves of LN-400-P-350 in 1.0 M KOH without and with 10 mM FOL.

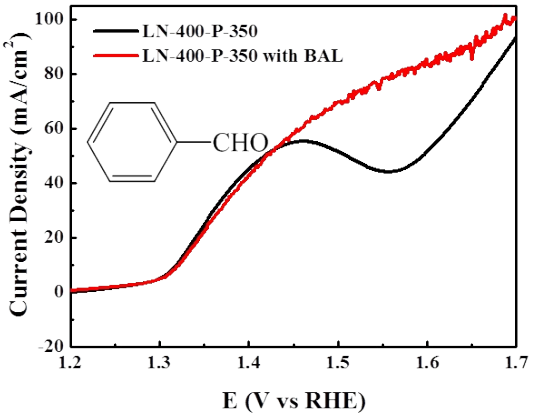

Fig. S11. LSV curves of LN-400-P-350 in 1.0 M KOH without and with 10 mM BAL.

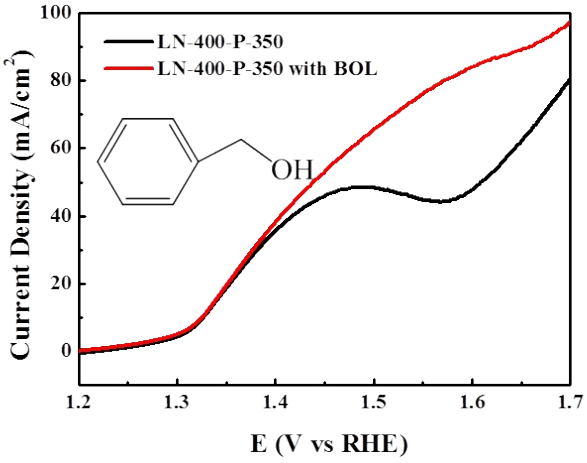

Fig. S12. LSV curves of LN-400-P-350 in 1.0 M KOH without and with 10 mM BOL.

Table S1. Comparisons of catalytic performance for the oxidation of HMF to FDCA over Ni-based and noble metal catalysts.

Catalysts	C_{HMF} (mM)	Time (min)	Potential (V vs RHE)	Conv. (%)	FDCA yield (%)	FE. (%)
NiCoFe-LDHs[1]	10	60	1.52	95.5	84.9	90
NiFe-LDH[2]	10	600	1.23	99	98	99.4
NiB_x@NF[3]	10	100	1.64	99.8	> 99	99
$NiCo_2O_4$[4]	5	53	1.43	99.6	90.8	87.5
Ni_2P/NF[5]	10	--	1.423	100	100	98
Ni_2S_3/NF[6]	10	--	1.423	98	98	100
Ni_3N@C[7]	10	--	1.45	100	98	99
NiCoBDC-NF[8]	10	240	1.55	--	99	78.8
1.0 h-$Ni(OH)_2$[9]	40	200	--	98.8	97.3	94.9
NiOOH[10]	5	282	1.47	99.8	96	96
NiOOH[11]	5	318	1.50	100	93.3	93.3
Pd_2Au_1/C[12]	20	60	0.9	100	64	--
Ir-Co_3O_4[13]	50	--	1.42	100	98	98
This work	10	45	1.49	100	> 99	> 90

References

1. M. Zhang, Y. Liu, B. Liu, Z. Chen, H. Xu and K. Yan, *ACS Catal.*, 2020, **10**, 5179-5189.
2. W.-J. Liu, L. Dang, Z. Xu, H.-Q.Yu, S. Jin and G. W. Huber, *ACS Catal.*, 2018, **8**, 5533−5541.
3. P. Zhang, X. Sheng, X. Chen, Z. Fang, J. Jiang, M. Wang, F. Li, L. Fan, Y. Ren, B. Zhang, B. J. J. Timmer, M. S. G. Ahlquist and L. Sun, *Angew. Chem. Int. Ed.*, 2019, **58**, 9155-9159.
4. M. J. Kang, H. Park, J. Jegal, S. Y. Hwang, Y. S. Kang and H. G. Cha, *Appl. Catal., B.*, 2019, **242**, 85-91.
5. B. You, N. Jiang, X. Liu and Y. Sun, *Angew. Chem. Int. Ed.*, 2016, **55**, 9913-9917.
6. B. You, X. Liu, N. Jiang and Y. Sun, *J. Am. Chem. Soc.*, 2016, **138**, 13639–13646.
7. N. Zhang, Y. Zou, L. Tao, W. Chen, L. Zhou, Z. Liu, B. Zhou, G. Huang, H. Lin and S.Wang, *Angew. Chem. Int. Ed.*, 2019, **58**, 15895-15903.

8. M. Cai, Y. Zhang, Y. Zhao, Q. Liu, Y. Li and G. Li, *J. Mater. Chem. A.*, 2020, **8**, 20386-20392.
9. X. Chen, X. Zhong, B. Yuan, S. Li, Y. Gu, Q. Zhang, G. Zhuang, X. Li, S. Deng and J.-G. Wang, *Green Chem.*, 2019, **21**, 578-588.
10. B. J. Taitt, D.-H. Nam and K.-S. Choi, *ACS Catal.*, 2018, **9**, 660-670.
11. J. Woo, B. C. Moon, U. Lee, H.-S. Oh, K. H. Chae, Y. Jun, B. K. Min and D. K. Lee, *ACS Catal.*, 2022, **12**, 4078-4091.
12. D. J. Chadderdon, L. Xin, J. Qi, Y. Qiu, P. Krishna, K. L. More and W. Li, *Green Chem.*, 2014, **16**, 3778-3786.
13. Y. Lu, T. Liu, C. L. Dong, Y. C. Huang, Y. Li, J. Chen, Y. Zou and S. Wang, *Adv. Mater.*, 2021, **33**, 2007056.